

Application of Compressive Sensing to Atmospheric Observations with Imaging Radar

Serkan Ozturk^{1,2,*}, Tian-You Yu^{1,2,3}, Lei Ding¹, Nai Feng^{1,2}, Boon Leng Cheong²

¹ School of Electrical and Computer Engineering, University of Oklahoma, Norman, Oklahoma, USA

² Advanced Radar Research Center, University of Oklahoma, Norman, Oklahoma, USA

³ School of Meteorology, University of Oklahoma, Norman, Oklahoma, USA

1. INTRODUCTION

In order to improve the understanding of the dynamics and structure of tornadoes or weather systems, fast scanning time is required for weather radars (Bluestein et al., 2003; Carbone et al., 1985). However, radar scan time for a volume coverage pattern (VCP) is constrained by the mechanical limitation of pedestal (Yu et al., 2007). On the other hand, the field of atmospheric reflectivity can be obtained by steering a pencil beam through the region of interest either mechanically from conventional weather radar with a dish antenna or electronically from phased-array antenna.

Phased array radars (PAR) were used for weather observations to achieve high data quality with a rapid scanning via beam multiplexing (Yu et al., 2007; Zrnic et al., 2007). Similar to phase array radars, imaging radars can provide high temporal resolution using digital beam forming (DBF) technique. In other words, multiple receiving beams are formed simultaneously within the field of view (FOV) by exploiting the phase differences of signals from a number of spatially separated arrays of antenna (Skolnik, 2001). The FOV is defined by the transmitted beam width, which is typically wide enough to cover the region of interest. No physical beam-steering is needed for imaging radar and all the beams are formed in the digital domain after signals received from multiple antenna arrays. Therefore, the scan time is significantly reduced because it is only determined by the dwell time. Moreover, an Atmospheric Imaging Radar (AIR) developed in the Advanced Radar Research Center (ARRC) of the University of Oklahoma. AIR transmits a fan beam width 20 degree in elevation and one de-

gree in azimuth and consists of 36 spatially separated receivers (Isom et al., 2013).

Imaging radar was used for observations of ionosphere with equatorial electrojet at top of the Jicamarca Radio Observatory (Kudeki and Sürücü, 1991) and reported that it also has the advantage of adaptive spatial clutter filtering, flexible update time at different beam positions and ranges, etc (Le et al., 2009; Yeary et al., 2011; Isom et al., 2013; Cheong et al., 2006). Further, coherent radar imaging is introduced based on constrained optimization using Capon's method for the lower atmosphere (Palmer et al., 1998). It has shown that Capon's method achieves higher angular resolution compared to Fourier beamforming (Palmer et al., 1998; Cheong et al., 2004). Recently, radar imaging has been considered as inverse scattering problem for the spatial map of reflectivity. Note that the number of receivers are much smaller than the number of angular sampling points on reflectivity field.

In this work, an emerging technology of compressive sensing (CS) is applied to measure the reflectivity field within the FOV of imaging radar. CS was developed to recover a sparse signal or an image with much fewer measurements than those normally required (Candès and Romberg, 2006; Donoho, 2006; Candès and Wakin, 2008). CS has been applied to many fields such as medical imaging (Lustig et al., 2007), radar waveforms (Baraniuk, 2007; Herman and Strohmer, 2009), etc. Moreover, CS is applied to estimate the direction of arrival (DOA) for multiple sources by using array sensors (Gurbuz et al., 2007; Wang et al., 2011). Also, an application of CS to beam forming for under water acoustic data is presented for finer angular resolution in (Edelmann and Gaumond, 2011).

It is important to note that the application of CS to DOA estimation, so far, was made pulse based (Gur-

* Corresponding author address: Serkan Ozturk, University of Oklahoma, 120 David L. Boren Blvd., Rm 5310, Norman, OK 73072-7307; e-mail: serkanozturk@ou.edu

buz et al., 2007; Wang et al., 2011; Edelmann and Gaumont, 2011). However, the computational time of CS is expensive for pulse based reconstruction. In this work, we develop a correlation based CS for reflectivity estimation with the goal of higher angular resolution. Both CS and Capon were implemented for the estimation of reflectivity field by using the array configuration based on AIR. Preliminary results have shown that CS can achieve higher angular resolution compared to Capon beamforming. The remainder of this paper is organized as follows. In section 2, formulation of beamforming will be briefly reviewed. A review of proposed compressive sensing algorithm and correlation based CS in section 3. Numerical simulation of reflectivity from imaging radar is shown in section 4. Statistical analysis of CS and Capon beamforming with results will be in section 5. The summary is presented in section 6.

2. FORMULATION OF BEAMFORMING

The reflectivity field for distinct angular directions can be estimated by combining received signal coherently from a given uniformly spaced phase arrays. The phased arrays are located with a certain distance to obtain phase shifts in order to steer the beam for different angular directions. By changing the weights for desired angles, a full map of reflectivity can be obtained within the transmitted beam of the radar. Let $\mathbf{x}(t)$ represent a vector of received signals at time t from M receivers. Then the received signal can be expressed in discrete and linear form for reflectivity as:

$$\mathbf{x}(t) = \mathbf{W}\mathbf{A} \quad (1)$$

where \mathbf{A} is reflectivity field and expressed independently from time for simplicity. \mathbf{W} is a measurement matrix or weighting matrix for beamforming. Practically, the received signals are obtained from continuous reflectivity field. For the sake of reconstruction and simplicity, let us assume that the reflectivity field \mathbf{A} is discretized to L number of angular points, $\mathbf{A} = [A(\theta_1), A(\theta_2), \dots, A(\theta_L)]^T$. Therefore, a set of pointing vectors is developed for L desired angles to estimate reflectivity field, creating a matrix \mathbf{W} .

$$\mathbf{W} = \begin{pmatrix} e^{jksin\theta_1 d_1} & e^{jksin\theta_2 d_1} & \dots & e^{jksin\theta_L d_1} \\ e^{jksin\theta_1 d_2} & e^{jksin\theta_2 d_2} & \dots & e^{jksin\theta_L d_2} \\ \vdots & \vdots & \dots & \vdots \\ e^{jksin\theta_1 d_M} & e^{jksin\theta_2 d_M} & \dots & e^{jksin\theta_L d_M} \end{pmatrix} \quad (2)$$

where k equals to $2\pi/\lambda$, d_m is the distance from m^{th} array to the center array $m = 1, 2, \dots, M$, λ is the radar wavelength and θ_l is desired angular directions $l = 1, 2, \dots, L$. For a particular angular direction, \mathbf{w} is obtained from l^{th} column of \mathbf{W} , $\mathbf{w} = \mathbf{W}_l$. As result, the size of matrix \mathbf{W} becomes $M \times L$. Typically, the number of receivers M is much smaller than L . Therefore, the reflectivity retrieval becomes an underdetermined inverse problem.

2.1. Fourier beamforming

The output of the beamformer, $\mathbf{y}(t)$, can be obtained by assigning a weighting vector, \mathbf{w} , for desired angular direction in the following:

$$\mathbf{y}(t) = \mathbf{w}^H \mathbf{x}(t) \quad (3)$$

where H is the Hermitian (complex conjugate) operator. The reflectivity field can be derived from the autocorrelation function of $\mathbf{y}(t)$ by assuming it is zero mean since the steering vector \mathbf{w} is data independent. Then the returned power from a particular direction can be obtained as following (Isom et al., 2013; Palmer et al., 1998):

$$P_F(\theta_l) = E[y(t)y^H(t)] = \mathbf{W}_l^H \mathbf{R}(0) \mathbf{W}_l \quad (4)$$

where $R(0) = E[x(t)x^H(t)]$. Fourier beamforming is only a function of direction and lead to constructive interference in the steering angle direction. The resolution is limited by the response of \mathbf{W} .

2.2. Capon beamforming

In order to improve angular resolution as minimizing the sidelobe effects, an adaptive weighting vector is obtained by constraining the weighting vector in the desired angle to minimize the output power (Isom et al.,

2013; Palmer et al., 1998; Cheong et al., 2006).

$$\min P(\theta_l) \text{ subject to } \mathbf{e}_l^H \mathbf{w} = 1 \quad (5)$$

Langrange method is performed to obtain output power (Isom et al., 2013; Palmer et al., 1998; Cheong et al., 2006) and the resulting form of the retuned power is given here.

$$P_C(\theta_l) = \frac{1}{\mathbf{W}_l^H \mathbf{R}(\mathbf{0})^{-1} \mathbf{W}_l} \quad (6)$$

It has shown that Capons method achieves higher angular resolution compared to Fourier beamforming. However, small errors present in the steering vector that can reduce the accuracy of amplitude estimations. Note that Capon weight vector was derived to minimize output power of beamformer subject to unity gain in the desired direction. No attempt was made to mitigate any noise effect on the estimation

3. COMPRESSIVE SENSING

The emerging theory of CS has been studied as a new framework for solving underdetermined problems in a linear model (Candès and Romberg, 2006; Donoho, 2006). It has been shown in CS that sparse images or signals can be reconstructed accurately from a limited number of incoherent measurements using nonlinear reconstruction (Candès and Romberg, 2006). In this paper, CS is applied to solve the inverse problem of reflectivity from phase array radar, where the number of receivers are less than number of angular points. In order to produce satisfactory reconstruction, CS requires three key elements such as sparsity, incoherence and l_1 -norm minimization.

Sparsity can be defined in either original domain or it transform domain that a signal can be represented by only a few nonzero coefficients. For example, if a signal has all pixels of nonzero values, it might only contain a few nonzero coefficients after a linear transformation, such as Fourier transform or wavelet. Practically, the condition of sparsity might not be met, but most of the natural signals can be compressible. The compressible means that the signal can be represented a few large

coefficients after transformation, but the rest of the coefficients have relatively smaller values.

In order to reconstruct sparse or compressible signals using CS, the measurements should be obtained incoherently. The coherence measures the similarity between the columns of the measurement matrix if the identity transformation is used. The lower coherence indicates that the less number of measurements needed for accurate reconstruction. Also, coherence can be used to guarantee stable reconstruction through l_1 -norm recovery. Consequently, the l_1 -norm tends to generate sparse solutions by penalizing small values heavily compared to l_2 -norm and it is defined as sum of the absolute values of the coefficients. Since the sparse signals have small l_1 -norm relative to the l_2 -norm, l_1 -norm is more efficient to retrieve sparse signals.

3.1. Formulation of correlation based CS

CS requires a linear relationship between the received signals and desired to estimate of reflectivity field. In this work, the goal for CS is to estimate power of reflectivity directly from correlation matrix. Therefore, in order to derive power equation for correlation based CS, autocorrelation of received signal is exploited in the following.

$$E[\mathbf{x}(\mathbf{t})\mathbf{x}^H(\mathbf{t})] = E[\mathbf{W}\mathbf{A}\mathbf{A}^H\mathbf{W}^H] \quad (7)$$

$$\mathbf{R}(\mathbf{0}) = \mathbf{W}E[\mathbf{A}\mathbf{A}^H]\mathbf{W}^H \quad (8)$$

Where \mathbf{W} is called as a measurement matrix for CS and to distinguish from the steering vector. It is assumed that the expectation of reflectivity for cross correlation equals to zero because the reflectivity is spatially uncorrelated for different sampling angles. The expectation of power of reflectivity is expressed in the following:

$$E[\mathbf{A}\mathbf{A}^H] = \begin{pmatrix} |A(\theta_1)|^2 & 0 & \dots & 0 \\ 0 & |A(\theta_2)|^2 & \dots & 0 \\ \vdots & \vdots & \dots & \vdots \\ 0 & 0 & \dots & |A(\theta_L)|^2 \end{pmatrix} \quad (9)$$

The squared term of reflectivity is expressed in a column vector and extracted from multiplication of the measurement matrices, $\hat{\mathbf{A}} = [|A(\theta_1)|^2, |A(\theta_2)|^2, \dots, |A(\theta_L)|^2]^T$.

Similarly, $\mathbf{R}(\mathbf{0})$ is also expressed in a column vector with the same order of $\hat{\mathbf{A}}$, denoted as $\hat{\mathbf{R}} = [R(1, 1), R(1, 2), \dots, R(2, 2), R(2, 3), \dots, R(M, M)]^T$. Note that only the upper triangle of $\mathbf{R}(\mathbf{0})$ is used for correlation based CS because of the lower triangle part is conjugate of the upper part and there is no new information. Subsequently, a linear relationship is derived for power of reflectivity from autocorrelation and correlated measurement matrix.

$$\hat{\mathbf{R}} = \mathbf{K}\hat{\mathbf{A}} \quad (10)$$

where \mathbf{K} is correlation measurement matrix and derived from 8,

$$\mathbf{K} = \begin{pmatrix} e^{jksin\theta_1(d_1-d_1)} & e^{jksin\theta_2(d_1-d_1)} & \dots & e^{jksin\theta_L(d_1-d_1)} \\ e^{jksin\theta_1(d_1-d_2)} & e^{jksin\theta_2(d_1-d_2)} & \dots & e^{jksin\theta_L(d_1-d_2)} \\ \vdots & \vdots & & \vdots \\ e^{jksin\theta_1(d_2-d_2)} & e^{jksin\theta_2(d_2-d_2)} & \dots & e^{jksin\theta_L(d_2-d_2)} \\ e^{jksin\theta_1(d_2-d_3)} & e^{jksin\theta_2(d_2-d_3)} & \dots & e^{jksin\theta_L(d_2-d_3)} \\ \vdots & \vdots & & \vdots \\ e^{jksin\theta_1(d_M-d_M)} & e^{jksin\theta_2(d_M-d_M)} & \dots & e^{jksin\theta_L(d_M-d_M)} \end{pmatrix} \quad (11)$$

As a result, the power of reflectivity retrieval using CS is obtained by solving the following minimization problem:

$$\min \|\tilde{\mathbf{A}}\|_{l_1} \quad \text{subject to} \quad \|\hat{\mathbf{R}} - \mathbf{K}\tilde{\mathbf{A}}\|_{l_2} < \epsilon \quad (12)$$

where ϵ controls the consistency between the estimated data from reconstruction and measured data. In other words, the retrieved reflectivity would be the sparsest solution among all solutions that are consisted with the acquired data.

4. NUMERICAL SIMULATIONS

Numerical simulations were developed to demonstrate and verify the feasibility of CS for reflectivity retrieval from imaging radar. The model reflectivity is simulated by using a three dimensional radar simulator to generate raw time series data for weather radar (Cheong et al., 2008). A field of thousands of scatterers is populated within the FOV of the radar. Simulator produces time series by adding coherently thousands of discrete signal by using the numerical weather parameters from Advanced Regional Prediction System (ARPS). For the

simulation, 36 receivers are used with the spacing $d = \lambda/2$. The simulation domain used for reflectivity simulation was -1.88 km to 1.88 km and with 50 m range gate. It is assumed that frequency of radar is 9.55 GHz and 20 dB transmitted beam width.

In this work, two Gaussian models with zero mean were considered to evaluate performance for resolution. It is assumed that the model reflectivity is 9 km ahead of the radar. Mean of the two Gaussian peaks are located at range $R_1 = 0km$ and $R_2 = 1.1km$ and standard deviation σ changes from 53.16 m to 265.8 m with every 35.44 m. In the reconstruction, 120 number of angular points are used between -12 degree to 12 degree.

5. NUMERICAL RESULTS

The goal this section is to investigate the performance of CS for different amounts of noise and various reflectivity structures through statistical analysis. Additionally, the performance of CS will be compared to Capon beamforming under these conditions. For each case 50 realizations were performed, each with independent noise sequence for various models, where signal to noise ratio (SNR) is used as 10 dB and 20 dB. The performance of CS reconstruction and Capon beamforming for the resolution are quantified by the resolution equation defined in (13). The resolution is defined as a local minimum exist between two peaks. The local minimum range is found between two symmetric peaks, $R_m = (R_1 + R_2)/2$. The two peaks in the Gaussian model are located at ranges R_1 and R_2 , which are the mean of the model peaks. The resolution of the estimated reflectivity field and model field was calculated in the following equation (Mir and Carlson, 2012).

$$res = \frac{1}{2}(P_{R_1} + P_{R_2}) - P_{R_m} \quad (13)$$

where (P_R is the power in logarithmic domain. Therefore, it corresponds the ratio of (P_{max}/P_{min}) in numerical scale for range $R_{1,2}$ and R_m .

5.1. SNR = 20 dB

The reflectivity was estimated by CS and Capon beamforming with 36 measurements and SNR = 20 dB in Fig-

ure 1. It is evident that both CS and Capon estimates

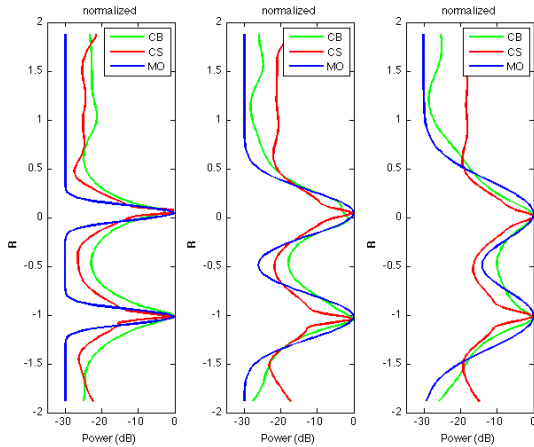


Figure 1: SNR=20dB. Gaussian model with two peaks (blue), CS reconstruction (red), Capon beamforming (green) and standard deviation of models, $\sigma=53.16$ m (left panel), $\sigma=159.49$ m (middle panel), $\sigma=159.49$ m (right panel)

mostly reflectivity changes for various standard deviation as shown in Figure 1. Also, Both CS and Capon are able to resolve the peaks, while CS has better separation than Capon by considering the lower dip at range R_m shown in the left and the middle panels of figure 1. On the other hand, when the standard deviation or midpoint amplitude at range R_m increases, the background level of CS increases as Capon sidelobes stay lower. On the other hand, the beam width in the CS reconstruction is narrower than Capon's. One of the reason is that the l_1 -norm minimization tends to sparse peak in the reconstruction since the simulated signals are Gaussian distributed which is more favored by l_2 -norm based solutions.

The mean resolution from CS and Capon as a function of standard deviation, σ , are shown in Figure 2. It is obvious that separation of two Gaussian models in CS reconstruction is better than Capon beamforming in Figure 2. Note that the higher resolution indicates the better separation between the peaks. Both of CS and Capon resolution reduce with the increasing the standard deviation since the peaks becomes closer in Figure 2 and 4. CS reconstruction has closer resolution to the model than Capon for all the cases in Figure 2.

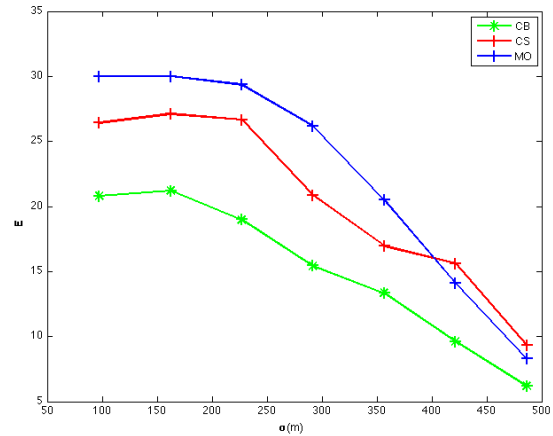


Figure 2: Resolution of Model (blue), CS reconstruction (red), Capon beamforming (green) with SNR=20 dB. Standard deviation of models changes from 53.16 m to 265.8 m every 35.44 m

5.2. SNR = 10 dB

CS and Capon are still able resolve the two peaks when the amount of noise increased to SNR=10 dB, while CS reconstruction has lower dip than Capon beamforming between the two peaks in Figure 3. For SNR=10 dB, the background level of the model above the 0.5 km, CS background level and Capon sidelobes are similar shown in the middle and right panel of Figure 3. By doing a cross comparison between the SNR=20 dB and SNR=10dB in Figures 1 and 3, both CS and Capon power estimation are reduced around 5 dB in SNR=10dB .

The amount of noise increased and SNR is set to 10 dB. The resolution of CS retrieval and Capon beamforming decreases as σ increases in Figure 4. Both CS and Capon beamforming resolve the peaks grossly. CS retrieval has closer resolution to the model than Capon beamforming with SNR=10 dB in Figure 4. Both CS and Capon resolution with SNR=10dB decreases comparing to resolution with SNR=20dB in Figures 2 and 4.

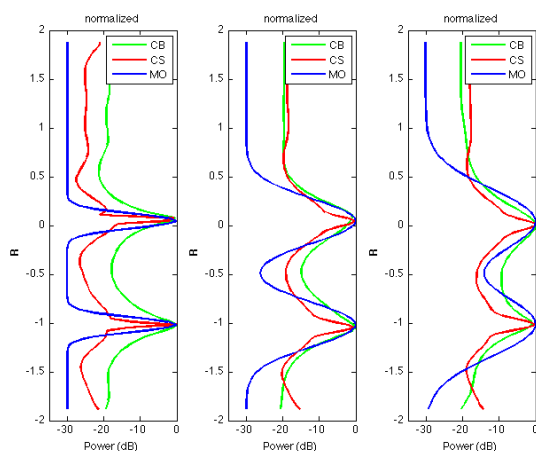


Figure 3: SNR=10dB. Gaussian model with two peaks (blue), CS reconstruction (red), Capon beamforming (green) and standard deviation of models, $\sigma=53.16$ m (left panel), $\sigma=159.49$ m (middle panel), $\sigma=159.49$ m (right panel)

6. SUMMARY

In this work, the application of CS to atmospheric observations using imaging radar was demonstrated. Performance of CS and Capon beamforming was evaluated statistically and compared using resolution metric. It is evident that CS and Capon are able to resolve the peaks consistently, while CS has better resolution than Capon for SNR=20dB and 10 dB. The results suggest that CS has potential to resolve close peaks better than Capon for the given conditions.

References

- Baraniuk, R., 2007: Compressive radar imaging. *Proc. IEEE Radar Conf.*, 128–133.
- Bluestein, H. B., W.-C. Lee, M. Bell, C. C. Weiss, and A. L. Pazmany, 2003: Mobile doppler radar observations of a tornado in a supercell near bassett, nebraska, on 5 june 1999. part ii: Tornado-vortex structure. *Monthly Weather Review*, **131**, 2968–2984.
- Candès, E. J. and J. Romberg, 2006: Sparsity and incoherence in compressive sampling.

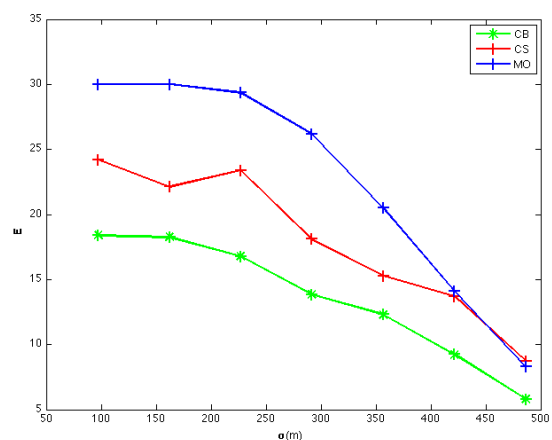


Figure 4: Resolution of Model (blue), CS reconstruction (red), Capon beamforming (green) with SNR=10 dB. Standard deviation of models changes from 53.16 m to 265.8 m every 35.44 m

- Candès, E. J. and M. B. Wakin, 2008: An introduction to compressive sampling. *IEEE Signal Process. Mag.*, **25**, 21–30.
- Carbone, R. E., M. J. Carpenter, and C. D. Burghart, 1985: Doppler radar sampling limitations in convective storms. *J. Atmos. Oceanic Technol.*, **2**, 357–361.
- Cheong, B. L., M. W. Hoffman, and R. D. Palmer, 2004: Efficient atmospheric simulation for high-resolution radar imaging applications. *J. Atmos. Oceanic Technol.*, **21**.
- Cheong, B. L., M. W. Hoffman, R. D. Palmer, S. J. Frasier, and F. J. López-Dekker, 2006: Phased-array design for biological clutter rejection: Simulation and experimental validation. *J. Atmos. Oceanic Technol.*, **23**, 585–598.
- Cheong, B. L., R. D. Palmer, and M. Xue, 2008: A time series weather radar simulator based on high-resolution atmospheric models. *J. Atmos. Oceanic Technol.*, **25**, 230–243.
- Donoho, D. L., 2006: Compressed sensing. *IEEE Trans. Inf. Theory*, **52**, 1289–1306.
- Edelmann, G. F. and C. F. Gaumont, 2011: Beamforming using compressive sensing. *J. Acoust. Soc. Am.*, **130**, EL232–EL237.

- Gurbuz, A. C., J. McClellan, and W. Scott, 2007: Compressive sensing for gpr imaging. *Signals, Systems and Computers, 2007. ACSSC 2007. Conference Record of the Forty-First Asilomar Conference on*, 2223–2227.
- Herman, M. A. and T. Strohmer, 2009: High-resolution radar via compressed sensing. *IEEE Trans. Signal Process.*, **57**, 2275–2284.
- Isom, B., R. Palmer, R. Kelley, J. Meier, D. Bodine, M. Yeary, B.-L. Cheong, Y. Zhang, T.-Y. Yu, and M. I. Biggerstaff, 2013: The atmospheric imaging radar: Simultaneous volumetric observations using a phased array weather radar. *J. Atmos. Oceanic Technol.*, **30**, 655–675.
- Kudeki, E. and F. Sürücü, 1991: Radar interferometric imaging of field-aligned plasma irregularities in the equatorial electrojet. *Geophysical Research Letters*, **18**, 41–44.
- Le, K., R. Palmer, B. L. Cheong, T.-Y. Yu, G. Zhang, and S. Torres, 2009: On the use of auxiliary receive channels for clutter mitigation with phased array weather radars. *Geoscience and Remote Sensing, IEEE Transactions on*, **47**, 272–284.
- Lustig, M., D. Donoho, and J. M. Pauly, 2007: Sparse MRI: The application of compressed sensing for rapid MR imaging. *Magn. Reson. Med.*, **58**, 1182–1195.
- Mir, H. and B. Carlson, 2012: On the definition of radar range resolution for targets of greatly differing rcs. *Instrumentation and Measurement, IEEE Transactions on*, **61**, 655–663.
- Palmer, R. D., S. Gopalam, T.-Y. Yu, and S. Fukao, 1998: Coherent radar imaging using capon's method. *Radio Science*, **33**, 1585–1598.
- Skolnik, M. I., 2001: *Introduction to Radar Systems*. Number 772 pp, McGraw-Hill, 3rd edition edition.
- Wang, J., Z. Huang, and Y. Zhou, 2011: Direction-of-arrival estimation based on joint sparsity. *Sensors*, **11**, 9098–9108.
- Yeary, M., G. Crain, R. Kelley, J. Meier, Y. Zhang, R. Palmer, T.-Y. Yu, A. Zahrai, I. Ivic, C. Curtis, and R. Doviak, 2011: Phased array weather / multipurpose radar. *Aerospace and Electronic Systems Magazine, IEEE*, **26**, 12–15.
- Yu, T.-Y., M. B. Orescanin, C. D. Curtis, D. S. Zrnić, and D. E. Forsyth, 2007: Beam multiplexing using the phased-array weather radar. *J. Atmos. Oceanic Technol.*, **24**, 616–626.
- Zrnic, D. S., J. F. Kimpel, D. E. Forsyth, A. Shapiro, G. Crain, R. Ferek, J. Heimmer, W. Benner, T. J. McNellis, and R. J. Vogt, 2007: Agile-beam phased array radar for weather observations. *Bull. Amer. Meteor. Soc.*, **88**, 1753–1766.